Torque-coupled thermodynamic model for F_oF_1-ATPase

Guangkuo Ai
Beijing International Center for Mathematical Research and School of Mathematical Sciences, Peking University, Beijing 100871, People's Republic of China

Pengfei Liu
Applied and Computational Mathematics, California Institute of Technology, Pasadena, California 91125, USA

Hao Ge*
Beijing International Center for Mathematical Research and Biodynamic Optical Imaging Center, Peking University, Beijing 100871, People's Republic of China

(Received 31 May 2016; revised manuscript received 2 March 2017; published 23 May 2017)

F_oF_1-ATPase is a motor protein complex that utilizes transmembrane ion flow to drive the synthesis of adenosine triphosphate (ATP) from adenosine diphosphate (ADP) and phosphate (Pi). While many theoretical models have been proposed to account for its rotary activity, most of them focus on the F_o or F_1 portions separately rather than the complex as a whole. Here, we propose a simple but new torque-coupled thermodynamic model of F_oF_1-ATPase. Solving this model at steady state, we find that the monotonic variation of each portion's efficiency becomes much more robust over a wide range of parameters when the F_o and F_1 portions are coupled together, as compared to cases when they are considered separately. Furthermore, the coupled model predicts the dependence of each portion's kinetic behavior on the parameters of the other. Specifically, the power and efficiency of the F_1 portion are quite sensitive to the proton gradient across the membrane, while those of the F_o portion as well as the related Michaelis constants for proton concentrations respond insensitively to concentration changes in the reactants of ATP synthesis. The physiological proton gradient across the membrane in the F_o portion is also shown to be optimal for the Michaelis constants of ADP and phosphate in the F_1 portion during ATP synthesis. Together, our coupled model is able to predict key dynamic and thermodynamic features of the F_oF_1-ATPase *in vivo* semiquantitatively, and suggests that such coupling approach could be further applied to other biophysical systems.

DOI: 10.1103/PhysRevE.95.052413

I. INTRODUCTION

F_oF_1-ATPase, a rotary motor protein complex that utilizes the electrochemical energy stored in trans-membrane ion gradients to drive the synthesis of adenosine triphosphate (ATP), plays a critical role in the energy metabolism of living cells [1,2]. After decades of research [3,4], we now have a comprehensive understanding of the structure and function of the enzyme [5–10]. In *E.coli*, the enzyme consists of two portions (F_o and F_1) coupled together by a central rotary asymmetric shaft (γ) [Fig. 1(a)]. The F_o portion is membrane embedded, and contains two proton channels and 10–15 copies of proton carriers (Asp61) distributed on a c ring [5]. Ions flow through the membrane via a subunit of the F_o portion, rotating the γ shaft. The F_1 portion, on the other hand, sits on the intracellular side of the membrane, and contains three hexagonal catalytic sites ($\alpha_3\beta_3$) involved in the synthesis of ATP molecules. The F_1 portion alone without coupling to the F_o portion can catalyze the spontaneous hydrolysis of ATP. However, under cellular conditions where the ionic concentration outside the membrane is higher than that inside, the electrochemical potential difference results in an ionic flow that drives the F_o portion and the γ shaft to rotate in the direction of ATP synthesis [11].

While *in vitro* biochemical research [7,9–17] as well as theoretical efforts [5,18–26] have helped reveal the mechanistic basis of the enzyme's action, most existing modeling approaches are either focused on the sole F_1 in the *in vitro* experiment or couple the actions of the two portions in complicated ways [18,21,22], without integrating our understanding of the kinetics and thermodynamics of the enzyme complex as a whole *in vivo*.

Here, we propose a simple thermodynamic scheme to couple the separate models for the F_o and F_1 portions in an attempt to recapitulate the behaviors of the two portions *in vivo*. The comparison of our model to the *in vitro* uncoupled situation with constant external torque is considered. We find that the profiles of each portion's efficiency and power in the coupled model can possibly be very different from those predicted from the uncoupled models. Furthermore, we systematically analyze how sensitively the kinetics and thermodynamics of one portion depend on the reactants involved in the chemical reaction of the other portion. It illustrates that the power, efficiency, and Michaelis constants for ATP synthesis of the F_1 portion are quite sensitive to the proton gradient across the membrane, while the dynamics and thermodynamics of the F_o portion respond insensitively to concentration changes in the reactants of ATP synthesis. Our model semiquantitatively recapitulates key dynamic and thermodynamic features of the F_oF_1-ATPase *in vivo*, and suggests that such coupling approach could be further applied to other biophysical systems.

*haoge@pku.edu.cn

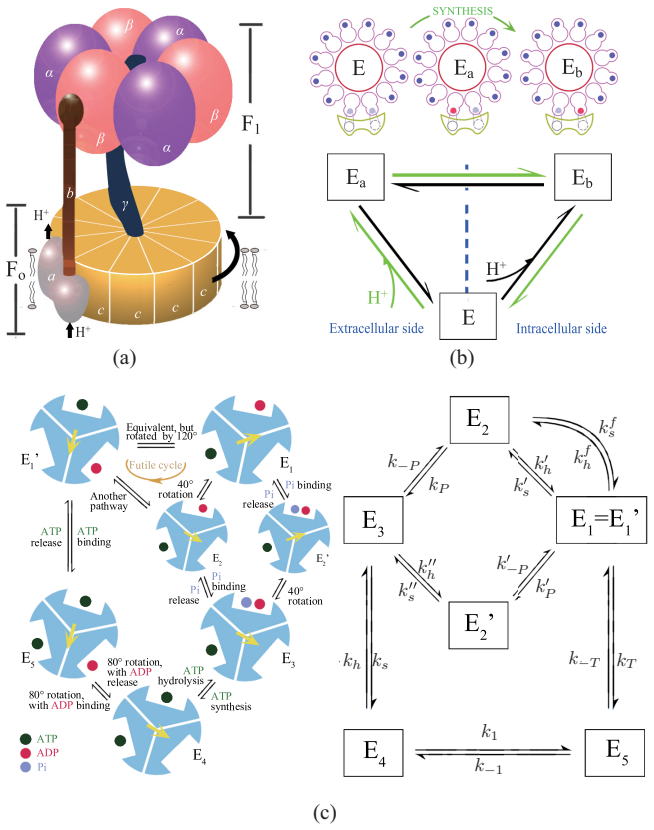

FIG. 1. Geometric structure and separate models for the F_o and F_1 portions. (a) Profile of the F_oF_1-ATP synthase structure, showing the two counter-rotating portions F_o and F_1 combined by an asymmetric shaft γ. F_o is membrane embedded, and F_1 is soluble in the cytoplasm. (b) Upper panel: Cross-sectional structure of F_o-ATPase, viewing from the extracellular side with its function illustrated. Filled dark and light circles represent whether protons bond to the carrier or not, respectively; the dashed circle represents one proton channel of the two which cannot be seen from this view. The free state E bonds to a proton from the extracellular side and becomes E_a. After clockwise rotation of F_o, the conformation E_a turns into E_b, which goes to again the initial state E by transferring the proton inside the intracellular side. (b) Lower panel: A discrete-state model of F_o, simplified from [27]. k_H is the second-order reaction constant. The sequence of events for protons entering the intracellular side of the membrane is shown by green (light gray) arrows, whereas the black arrows indicate the possibility in bringing out the protons from the intracellular side to the extracellular side. (c) Left panel: Discrete-state model of F_1, redrawn from [5,24]. For each ATP molecule to be synthesized (hydrolyzed), the γ shaft, shown as the dark yellow solid arrow, rotates 40 and 80° clockwise (anticlockwise) successively. (c) Right panel: The extraction from the left panel. Transition rates $k_\alpha, k_{-\alpha}$ are binding or dissociation rates for species $\alpha = D(\mathrm{ADP}), P(\mathrm{P_i}), T(\mathrm{ATP})$. The transition between states E_4 and E_5 includes the 80° rotation with reaction rates k_h''', k_s''' and the phosphate binding/releasing with k_D, k_{-D}, hence $k_1 = k_1(k_D, k_s''')$ and $k_{-1} = k_{-1}(k_{-D}, k_h''')$ [28]. After the completion of one cycle, the state E_1 turns to an equivalent state with the γ shaft rotating by 120°.

II. MODELS

Discrete-state models for the F_o portion (simplified from [27]) and F_1 portion (modified from [5,24]) are shown in Figs. 1(b) and 1(c). The average torque between the two portions is incorporated into the corresponding transition rates between different states in the models according to the thermodynamic principles. The two models are then coupled together based on Newton's third law, i.e., the average torques applied by one portion on the other are equal in magnitude and opposite in direction, leading to opposing effects on the rotary fluxes of the two portions.

A. Discrete-state models at nonequilibrium steady state

We begin our analysis by considering the cyclic chemical kinetics of a single molecule transiting among N discrete states forming a cycle in which only the transition between S_1 and S_2 can be coupled with mechanical work

$$S_1 \underset{k_{-1}^{\omega}}{\overset{k_1^{\omega}}{\rightleftharpoons}} S_2 \underset{k_{-2}}{\overset{k_2}{\rightleftharpoons}} \cdots \underset{k_{-(N-1)}}{\overset{k_{N-1}}{\rightleftharpoons}} S_N \underset{k_{-N}}{\overset{k_N}{\rightleftharpoons}} S_1,$$

for which the entropy production rate at steady state can be defined as

$$\mathrm{EPR} = J \cdot k_B \ln \frac{k_1^{\omega} k_2 \cdots k_N}{k_{-1}^{\omega} k_{-2} \cdots k_{-N}},$$

where J is the steady-state cycle flux [29,30], i.e., the average number of cycle occurrence per unit time.

We denote $\vec{\pi} = (\pi_1, \pi_2, \ldots, \pi_N)$ as the corresponding steady-state probability distribution among the N different states of the molecule and thus

$$J = k_1^{\omega}\pi_1 - k_{-1}^{\omega}\pi_2 = \cdots = k_N\pi_N - k_{-N}\pi_1.$$

Without any externally applied torque, the product of entropy production rate and the temperature gives the chemical free energy input per unit time [30,31]. Applying external torque can, however, alter the reaction rates of each step that is coupled to mechanical work. For example, if there is an amount of mechanical work W done during the transition from state S_1 to S_2, then we must have

$$\frac{k_1^{\omega}}{k_{-1}^{\omega}} = \frac{k_1^{\omega,0}}{k_{-1}^{\omega,0}} e^{\beta W},$$

where $k_1^{\omega,0}$ and $k_{-1}^{\omega,0}$ are the reaction rates between S_1 and S_2 without applied external torque and $\beta = \frac{1}{k_B T}$. This relation is a consequence of the conservation of energy, since the total free-energy dissipation (the product of entropy production rate and temperature) is simply the difference between the chemical free-energy input and the mechanical work output [29,30]. These general rules will be applied to the discrete-state models of both F_o and F_1 portions.

Moreover, we use a parameter δ, called the load distribution factor [23,32], with which we can rewrite the transition rates k_1 and k_{-1} as

$$k_1^{\omega} = k_1^{\omega,0} e^{\beta\delta W}, \quad k_{-1}^{\omega} = k_{-1}^{\omega,0} e^{-\beta(1-\delta)W}. \tag{1}$$

Here we provide a simple derivation of Eq. (1) from Kramers's rate formula [23,32–35]. Suppose that the transition between S_1 and S_2 is actually driven by the double-well potential $U(x)$ along the reaction coordinate $x \in [0, L]$, then $k_1^{\omega} \propto e^{-\beta[U(x^*)-U(0)]}$, in which x^* is the coordinate of the transition state and $U(x^*) - U(0)$ is the energy barrier from

S_1 to S_2. In the presence of external mechanical force $F(x)$, the resulting potential $U(x) = U_0(x) + \int_0^x F(s)ds$ where U_0 stands for the potential without external force. As such, the δ in Eq. (1) can be explicitly expressed as

$$\delta = \int_0^{x^*} F(x)dx \Big/ \int_0^L F(x)dx,$$

and the external work $W = \int_0^L F(x)dx = \bar{F} \cdot L$ (see [28] for more details). Therefore, the load distribution factor δ just reflects the distribution of the external work to the forward and backward transition rates. This derivation also implies that Eq. (1) does not depend on the assumption of constant torque, i.e., the force $F(x)$ can vary with the reaction coordinate x [36].

B. Discrete-state model of the F_o portion

Based on structural information, at least three different states, E, E_a, and E_b, are required for the c ring of F_o to function properly [Fig. 1(b)]. Two proton channels are shown in cyan (hollow) circles. E_a and E_b stand for the state bound by a proton entering the channel from the extracellular or intracellular side, respectively, while E stands for the proton-free state; the transition from E_a to E_b is simply achieved through a clockwise rotation. A discrete-state model of the F_o portion, simplified from [27], is shown in the lower panel in Fig. 1(b), in which k_H is the second-order reaction constant, and k_s^*,k_h^* are the transition rates between E_a and E_b. The green (light gray) arrows denote the sequence of events following the entrance of protons from the intracellular side of the membrane. A comparison of the simulated rotation rate versus load torque between this simplified model and the original model in Ref. [27] can be seen in Ref. [28].

Since the transition from the state E_a to E_b results in the rotation of the γ shaft and induces torque, the transition rates k_s^* and k_h^* can be assumed to be

$$k_s^* = k_s^{0*} e^{-\beta\delta W}, \quad k_h^* = k_h^{0*} e^{\beta(1-\delta)W}, \tag{2}$$

where δ is just the distribution factor, W is the work that the F_o portion does through the 30° rotation in the case of 12 c subunits, and k_s^{0*} and k_h^{0*} are the transition rates without external force, respectively. The external work W is given by

$$W = \bar{F}l = \bar{F} \times \frac{\pi}{6}r = \frac{\pi}{6}\bar{M},$$

where r is the radius of the γ shaft and $\bar{M}$ is the average torque.

We denote J_o as the rotation flux of F_o parallel to the direction of ATP synthesis, which can be expressed in terms of the Michaelis constants of the proton concentrations on both sides of the membrane as

$$J_o = \frac{V_a \frac{[H^+]_a}{K_{ma}} - V_b \frac{[H^+]_b}{K_{mb}}}{1 + \frac{[H^+]_a}{K_{ma}} + \frac{[H^+]_b}{K_{mb}}}, \tag{3}$$

where $[H^+]_a$ and $[H^+]_b$ are proton concentrations on the extracellular and intracellular sides, and the specific expressions of V_a,V_b as well as the Michaelis constants K_{ma}, K_{mb} dependent on all of the reaction rates of the F_o model are given in Ref. [28].

Subsequently, we have the power of F_o as

$$P_o = \frac{\pi}{6}\bar{M}J_o. \tag{4}$$

Meanwhile, the total free-energy change for a proton transported across the inner membrane is

$$\Delta G_o = \Delta\psi + \Delta\mu_H,$$

where $\Delta\psi = 140$ mV $= 5.6k_BT$ is a fixed membrane potential due to electrostatic force, and $\Delta\mu_H$ is the chemical potential caused by the transmembrane proton gradient. The total free-energy change also establishes a thermodynamic constraint for the reaction rates, which helps us to estimate the reaction rates in our model (see [28] for details).

Since ΔG_o is the free-energy input of the F_o portion, the thermodynamic efficiency of F_o can be obtained as

$$\eta_o = \frac{\pi\bar{M}}{6\Delta G_o} = \frac{\pi\bar{M}}{6\left(\Delta\psi + k_BT\ln\frac{[H^+]_a}{[H^+]_b}\right)}. \tag{5}$$

This thermodynamic efficiency attains its maximum 100% when the γ shaft meets its stall torque, at which the rotary flux is zero. It is a general property for a tightly coupled rotary molecular motor [14,23,32,33].

C. Discrete-state model of the F_1 portion

Among the many models proposed for the F_1 portion [1,5,6,18–22,24,32,37,38], here we choose to combine the models in Refs. [5,24] [Fig. 1(c)]. The F_1 portion begins its catalytic cycle from state E_1; after a 40° clockwise rotation of the shaft accompanied by phosphate binding, the portion adopts the E_3 conformation which, upon ATP synthesis, transits to state E_4. Subsequently, another clockwise rotation of the shaft by 80° accompanied by adenosine diphosphate (ADP) binding transits the portion to E_5, which then releases the ATP and returns the enzyme to E_1'. On the other hand, when ATP concentration is extremely low, the γ shaft may rotate 80° without undergoing ATP synthesis [39], suggesting an alternative "futile" pathway from E_2 to E_1'.

Similar to Eq. (2), we now have

$$\begin{aligned}
k_s' &= k_s'^0 e^{\frac{2\pi}{9}\beta(1-\delta')\bar{M}}, & k_s'' &= k_s''^0 e^{\frac{2\pi}{9}\beta(1-\delta'')\bar{M}},\\
k_h' &= k_h'^0 e^{-\frac{2\pi}{9}\delta'\bar{M}}, & k_h'' &= k_h''^0 e^{-\frac{2\pi}{9}\beta\delta''\bar{M}},\\
k_s''' &= k_s'''^0 e^{\frac{4\pi}{9}\beta(1-\delta''')\bar{M}}, & k_s^f &= k_s^{f,0} e^{\frac{4\pi}{9}\beta(1-\delta^f)\bar{M}},\\
k_h''' &= k_h'''^0 e^{-\frac{4\pi}{9}\delta'''\bar{M}}, & k_h^f &= k_h^{f,0} e^{-\frac{4\pi}{9}\delta^f\bar{M}},
\end{aligned} \tag{6}$$

where $k_s'^0$,$k_h'^0$,$k_s''^0$,$k_h''^0$ denote the rates of the 40° rotation steps and $k_s'''^0$,$k_h'''^0$,$k_s^{f,0}$,$k_h^{f,0}$ denote rates of the 80° rotation steps (all without external torque), and δ',δ'',δ''',δ^f are the corresponding load distribution factors described above. Denoting the invariant distribution of the model in Fig. 1(c) as $\bar{\pi} = (\pi_{E_1}, \cdots, \pi_{E_5})$, the expected rotary flux of F_1 for both ATP synthesis and the futile cycle in unit time can then be expressed in terms of these rates as

$$\begin{aligned}
J_1^e &= k_s\pi_{E_3} - k_h\pi_{E_4},\\
J_1^f &= k_s^f\pi_{E_2} - k_h^f\pi_{E_1}.
\end{aligned}$$

TABLE I. Parameter values of the model.[a]

Parameters from earlier work [20,24,27,43]			
$k_H = 1.11 \times 10^{11}\,\mathrm{M^{-1}\,s^{-1}}$	$k_{-H_a} = 2.15 \times 10^{4}\,\mathrm{s^{-1}}$	$k_{-H_b} = 5.8 \times 10^{6}\,\mathrm{s^{-1}}$	
$k_T = 2.5 \times 10^{6}\,\mathrm{M^{-1}\,s^{-1}}$	$k_D = 6 \times 10^{6}\,\mathrm{M^{-1}\,s^{-1}}$	$k_P = 1.7 \times 10^{5}\,\mathrm{M^{-1}\,s^{-1}}$	$k'_P = 4 \times 10^{5}\,\mathrm{M^{-1}\,s^{-1}}$
$k_{-T} = 90\,\mathrm{s^{-1}}$	$k_{-D} = 6 \times 10^{2}\,\mathrm{s^{-1}}$	$k_{-P} = 8 \times 10^{2}\,\mathrm{s^{-1}}$	$k'_{-P} = 1 \times 10^{7}\,\mathrm{s^{-1}}$
$k_h'^0 = 2 \times 10^{4}\,\mathrm{s^{-1}}$	$k_s'^0 = 40\,\mathrm{s^{-1}}$	$k_h''^0 = 1 \times 10^{2}\,\mathrm{s^{-1}}$	$k_s''^0 = 1 \times 10^{4}\,\mathrm{s^{-1}}$
$k_h = 4 \times 10^{3}\,\mathrm{s^{-1}}$	$k_h'''^0 = 1 \times 10^{4}\,\mathrm{s^{-1}}$	pH_a=7[b]	pH_b=8.4[b]
[PI] = 6 mM[c]	[ATP] = 4 mM[c]	[ADP] = 0.3 mM[c]	$T = 293\,\mathrm{K}$
Parameters estimated			
$k_s^{0*} = 5.1 \times 10^{3}\,\mathrm{s^{-1}}$	$k_h^{0*} = 5.1 \times 10^{3}\,\mathrm{s^{-1}}$	$k_s'''^0 = 1 \times 10^{2}\,\mathrm{s^{-1}}$	$k_s = 1 \times 10^{3}\,\mathrm{s^{-1}}$
$k_s^{f,0} = 5 \times 10^{-2}\,\mathrm{s^{-1}}$	$k_h^{f,0} = 1 \times 10^{-4}\,\mathrm{s^{-1}}$	$\delta = 0.35$	$\delta' = 0.6$
$\delta'' = 0.1$	$\delta''' = 0.8$	$\delta^f = 0.8$	

[a]Details for the estimation of parameter values and model consistency can be seen in Ref. [28].
[b]For *E.coli* the cytoplasmic pH_b is higher than the periplasmic pH_a [45]; these two parameter values are from [27].
[c]These parameter values are set to be in consistency with the aerobic living condition for *E.coli* in Ref. [43].

The total rotation rate of F_1 is therefore $J_1 = J_1^e + J_1^f$ (see [28] for details).

The chemical potential change associated with the synthesis or hydrolysis of one ATP molecule is

$$\Delta\mu_G = -\Delta G_{\mathrm{sol}} + k_B T \ln \frac{[T]}{[D][P]}, \tag{7}$$

which sets a thermodynamic relation between the reaction rates and the standard intrinsic free energy:

$$\Delta G_{\mathrm{sol}} = -50\ \mathrm{pN\,nm}.$$

The power of the F_1 portion for ATP synthesis can be described as $P_1 = J_1^e \Delta\mu_G$. Thus we have the efficiency of the F_1 portion to synthesize ATP:

$$\eta_1 = \frac{\Delta\mu_G}{\frac{2\pi}{3}\bar{M}} \times \frac{J_1^e}{J_1^e + J_1^f}. \tag{8}$$

Multiplying Eq. (8) with Eq. (5) yields the overall thermodynamic efficiency of the entire F_oF_1 complex, which is the ratio of free energy of ATP synthesis and the ionic gradient multiplied by the ratio of effective rotation rate of F_1 over its total rotation rate.

The Michaelis constants K_m of the reactants for the rotary flux J_1^e of F_1 for ATP synthesis are defined as their concentrations at which J_1^e is half of the maximum rate as the other reactants' concentrations are fixed. Detailed expressions are given in Ref. [28].

Using this model we calculated a 91% thermodynamic efficiency for the F_1 portion, in good agreement with the recent experimental work [40] using the same condition of 10-μM ATP, 10-μM ADP, and 1-mM Pi, lending support to the consistency of our model.

D. Coupling the two portions through torque

Under steady-state conditions in the cell where the F_o portion and F_1 portion are tightly coupled, we have

$$J_o = 4J_1. \tag{9}$$

This is because under the assumption of tight coupling between F_o and F_1, the completion of one rotation of F_o rotates the γ shaft by 30° while the completion of one rotation of F_1 rotates the γ shaft by 120°, in case there are 12 copies of proton carriers in F_o. However, in some cases the number of c subunits is not 12, or the tight coupling assumption is not valid, e.g., having slippage, we just need to modify the coefficient factor 4 in Eq. (9), e.g., 10/3 for the case with ten subunits of the c ring [41,42] or some certain ratio α between the average rotary velocities (fluxes) of F_o and F_1 *in vivo* at steady state.

Therefore, we can couple the F_o portion with the F_1 portion accordingly, regarding the average torque on the shaft as a function of all the concentrations of reactants and products. Such a coupled model regards the average torque on the shaft as a function of the concentrations of related chemical substances and reaction rates, in contrast to the *in vitro* situation in which the torque is externally applied and is either constant or just a direct correlate of the viscosity of the medium.

Table I gives all parameters used in the construction of the coupled model, some of which are obtained from earlier work directly [20,24,27,43] while others are estimated by fitting the model to known experimental measurements, such as the thermodynamic relation and rotation rate for each portion [18,44]. All concentrations of reactants or products are consistent with their physiological values reported previously [27,43], unless otherwise specified. It estimates the average torque at the value of 57.7 pN nm, which fits the previous estimation [27]. See [28] for the details of the coupled model.

III. RESULTS

Our coupled model allows a comparison between the *in vivo* and *in vitro* circumstances, and is capable of predicting the interdependence between the properties of the two portions, which cannot be revealed by models of sole F_o or F_1 portion. Below we give our results for the case of 12 c subunits; similar conclusions were obtained for the case of ten subunits or when using an alternative model of the F_1 portion [19], suggesting the robustness of all the results found in our coupled model [28].

A. Monotonicity of each portion's efficiency

The F_oF_1-ATPase transforms the electrochemical energy of a proton across the membrane to the free-energy difference

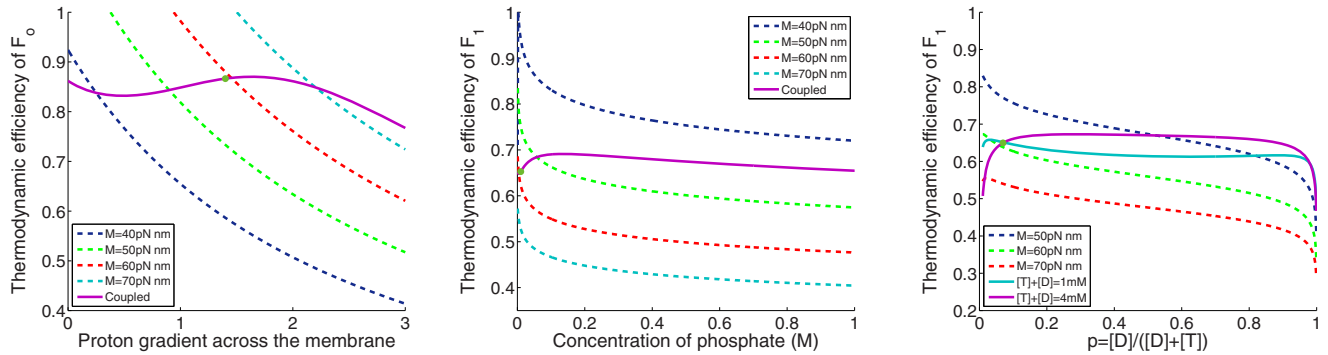

FIG. 2. Efficiency profiles for F_o and F_1 portions in coupled and uncoupled conditions. The profiles for the coupled situations are shown in solid lines; the green solid circle stands for the physiological condition. (a) Efficiency of F_o vs the proton gradient, with intracellular $\mathrm{pH}_b = 8.4$. In the uncoupled condition with fixed different values of the average torque M, the efficiency decreases with the increasing of the proton gradient; the coupled case leads to much slower decreasing, even becoming increasing at certain parameter ranges. The physiological condition ($\Delta\mathrm{pH} = 1.4$) gives the F_o portion's efficiency around 84.7%. (b), (c) Efficiency of F_1 vs phosphate concentration (with $[T] = 4\,\mathrm{mM}$, $[D] = 0.3\,\mathrm{mM}$) and the fraction of ADP over ADP plus ATP (with $[P] = 6\,\mathrm{mM}$), as the total concentration of ADP and ATP is fixed. The uncoupled condition gives a monotonically decreasing profile for the efficiency; in the coupled case, the decreasing of efficiency becomes much slower, even increasing at a certain parameter range. The physiological condition ($p = 0.07$) gives the F_1 portion's efficiency around 66%.

for ATP synthesis. Given that the electrochemical energy of the proton across the membrane is monotonically dependent on the intracellular and extracellular proton concentrations while the free energy for ATP synthesis is monotonically dependent on the concentrations of ATP, ADP, and phosphate, the efficiency of each portion under constant torque in the uncoupled case is also monotonically dependent on the concentrations of related chemical substances. However, such monotonicity is not obvious when the two portions are coupled.

In our coupled model (Fig. 2, the magenta curve), we show how the efficiency of the F_o portion is dependent on the pH difference across the membrane [see Fig. 2(a), with intracellular pH fixed], and how the efficiency of the F_1 portion is dependent on the concentration of phosphate and the ratio [ADP]/([ADP]+[ATP]) [see Figs. 2(b) and 2(c), with both intracellular and extracellular pHs fixed]. These efficiencies in the coupled model respond much more robustly than in the uncoupled case with constant external torque over a wide range of parameters; at certain parameter ranges the efficiency profiles even increase.

Under physiological conditions, the efficiency of the F_o calculated from our model is about 84.7% while that of the F_1 is about 66%, giving a total efficiency of 56.2% for the whole enzyme complex. It is worth mentioning that the extremely high efficiency of the F_1 measured *in vitro* [9,18,46] refers to the so-called Stokes efficiency rather than the thermodynamic efficiency [5] we calculate here.

In fact, the average torque on the shaft in our coupled model does not remain fixed, but rather increases with the increase in pH difference across the membrane and decreases with the increase of the phosphate concentration as well as the ratio [ADP]/([ADP]+[ATP]). Such a variation of the average torque as adjusting the concentrations of chemical substances results in the slowdown of the decreasing of efficiency compared to the *in vitro* case with constant torque (Fig. 2). In certain parameter ranges, the model predicts that variation in torque is even more significant than the variation in electrochemical potential of protons in the F_o portion, or in the free energy of ATP in the F_1 portion, leading to the unusual increase in each portion's efficiencies (Fig. 2).

B. Sensitivity of a separate portion's power and efficiency in the coupled model

We turn to the dependence of each portion's power and efficiency on the reactant concentrations of the other, a feature that can only be explored in such a coupled model. We find that the power and efficiency of F_o as well as the resulting average torque exhibit a gentle response to the variation of the reactant concentration in the F_1 portion, and are relatively stable over a quite wide parameter range [Figs. 3(a)–3(c), with intracellular and extracellular pHs fixed at physiological values].

On the other hand, the power and efficiency of F_1 as well as the resulting average torque are S shaped and sensitive to variations in the proton gradient: the power increases while the efficiency decreases with increasing proton gradient, with maximal slope around $\Delta\mathrm{pH} \sim 1.2$ [Fig. 3(d), with intracellular pH fixed and extracellular pH floating, and $[T],[D],[P]$ set to be at their physiological values].

In addition, since the rate of ATP production, i.e., the effective rotation rate of F_1 in the present model, is proportional to the power of F_1 as the chemical potential difference during the ATP synthesis is invariant when tuning the proton gradient across the membrane, the rate of ATP production is also S shaped and sensitive to variations in the proton gradient, with intracellular pH fixed and extracellular pH floating, and $[T],[D],[P]$ set to be at their physiological values. In order to avoid redundancy, we give the details in Ref. [28].

C. Michaelis constants of the reactants for the rotary flux

The coupled model also permits us to estimate the Michaelis constants for the reactants. After coupling with the F_1 portion, the Michaelis constants of the extracellular and intracellular protons for the rotary flux remain stable at around 0.197 and

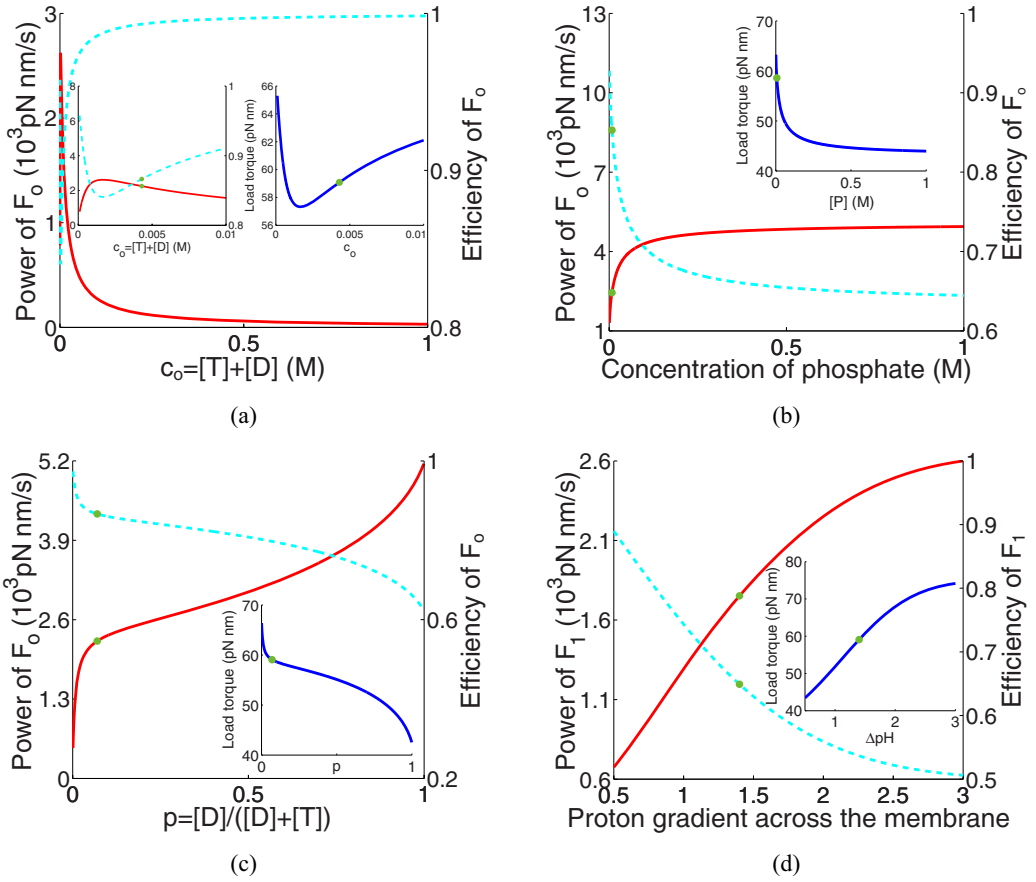

FIG. 3. The sensitivity of a separate portion's power and efficiency in the coupled model. In each figure the red (gray) and indigo (dashed light gray) lines stand for the power and efficiency profile, respectively, and the blue line embedded in each figure gives the torque on the shaft. (a)–(c) Power and efficiency of the F_o portion changing with the total concentration of ADP and ATP (with $p = 0.07$, $[P] = 6$ mM), the phosphate concentration (with $[T] = 4$ mM, $[D] = 0.3$ mM), as well as the ratio of ADP concentration (with $[T] + [D] = 4.3$ mM, $[P] = 6$ mM). The power and efficiency and the resulted average torque response stably when the tuned parameters are around their physiological values. A zooming-in subfigure for the profile with c_o ranging in [0, 0.01 mM] is inserted in (a). (d) Power and efficiency of the F_1 portion changing with the proton gradient, with $[T] = 4$ mM, $[D] = 0.3$ mM, $[P] = 6$ mM. The profiles of power, efficiency, and average torque are all S shaped with maximal slope at $\Delta\text{pH} = 1.2$.

2 μM, respectively, when tuning the phosphate concentration as well as the total concentration of ATP and ADP [Figs. 4(a) and 4(b)].

The Michaelis constants of ADP and phosphate for the rotary flux are both always deceasing with the proton gradient below $\sim$1.4 and increasing when the proton gradient is above $\sim$1.4 [Figs. 4(c) and 4(d), with intracellular pH fixed]. The response of the Michaelis constants of ADP with respect to the high proton gradient is much more smooth than that with respect to the low proton gradient.

The physiological value of the proton gradient across the membrane in the F_o portion is also found to be very close to the value at which the Michaelis constants of ADP and phosphate in the F_1 portion during ATP synthesis reach the minimum [Figs. 4(c) and 4(d)], suggesting a possible selection for the optimal value during evolution.

IV. DISCUSSION

Mathematical models have become more and more important for understanding the quantitative behaviors of a wide variety of biological systems ranging from a single molecule to large networks [47–51]. Particularly, in the scenarios that the *in vitro* experiments can only provide partial information on certain aspects of the system or that the *in vivo* measurements with the same resolution are not feasible, the thermodynamic consistent mathematical models can help to integrate the information on these disparate aspects from *in vitro* measurements to inform the functionally relevant behaviors of the system *in vivo*.

In the present paper, we use two separate stochastic models for the F_o and F_1 portions of the F_oF_1-ATPase, a key molecular machine involved in cellular energy metabolism, and couple them using the average torque between the two portions. The resulting torque-coupled model predicts a distinct behavior of monotonic variation of each portion's efficiency in the *in vivo* and *in vitro* situation, dependent on the relevant reactant concentrations, and reveals the mutual sensitivity of each portion's power and efficiency on the other. The invariance of these predicted behaviors with respect to the other existing models for the F_1 portion used in Ref. [28] demonstrates the robustness of our coupled model. The idea

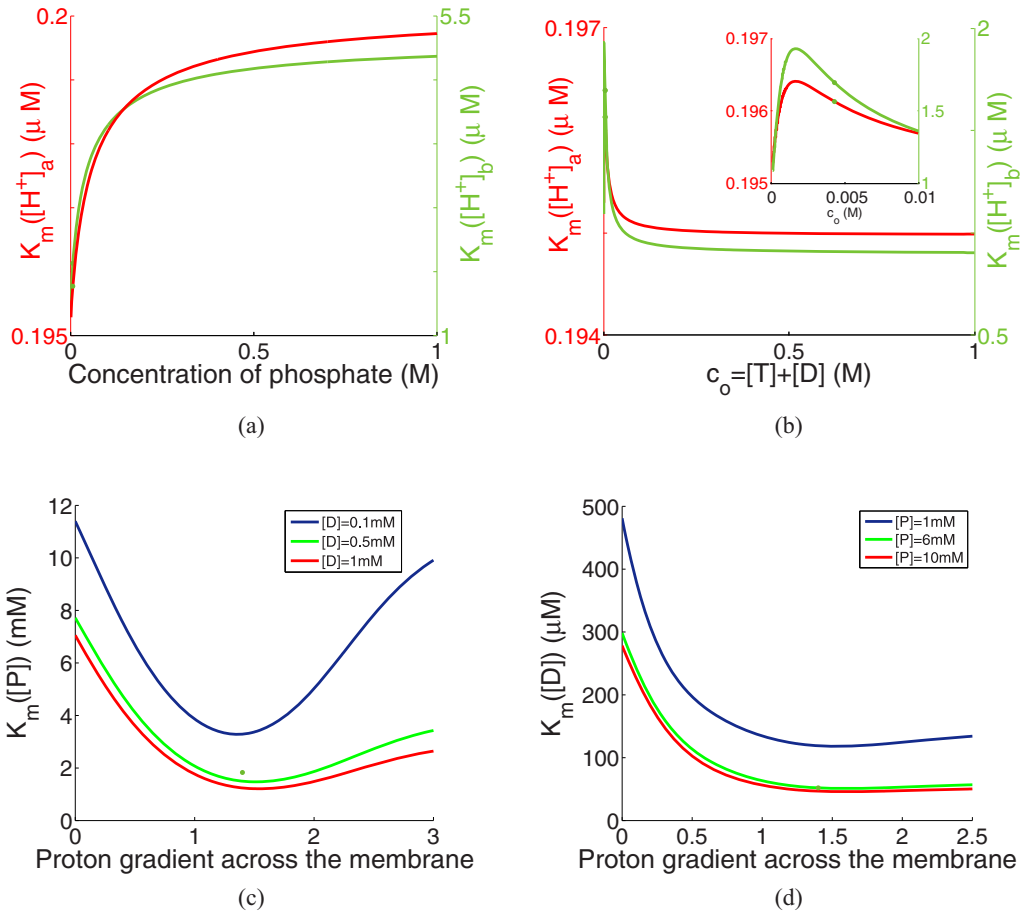

FIG. 4. Michaelis constants of the reactants for the rotary flux of the whole enzyme. (a), (b) $K_m([\mathrm{H}^+])$ depends on the phosphate concentration (with $[D] = 0.3$ mM, $[T] = 4$ mM) or the total concentration of ATP and ADP (with $[P] = 6$ mM, $p = 0.07$). In (a), the two constants, $K_m([H^+]_a)$ and $K_m([H^+]_b)$, reach a plateau even when $[P]$ is quite low, and remain stable at a certain range of $[P]$. In (b), the Michaelis constants are rather stable and there is a maximal value for both at $c_0 \sim 1.8$ mM. A zooming-in graph of the profile with c_o ranging in [0, 0.01 mM] is inserted. (c), (d) $K_m([P])$ and $K_m([D])$ depend on the proton gradient across the membrane with $[T] = 4$ mM and $\mathrm{pH}_b = 8.4$. The two curves shows their minimal value at around $\Delta\mathrm{pH} \sim 1.4$. When the proton gradient is high, the Michaelis constant can even increase.

of the coupling approach introduced in this paper can be further applied to a wide range of applications such as Myosin and bacterial flagellar motors [37], for which *in vivo* or *in vitro* measurements on individual parts are already available, but probing the complex as a whole remains unfeasible.

In our model, the expressions for the transition rates dependent on the average torque do not need the assumption of constant torque along the reaction coordinate, which is just a consequence of Kramers's rate formula. The case of mismatch between the number of c rings in F_o and the three components of F_1 can also be included into the model through the modification of Eq. (9) [28], since our coupled model is only investigated under steady-state conditions.

While the simple coupled model we present here is capable of capturing and predicting certain quantitative behaviors of the F_oF_1-ATPase, more improvement could be made by incorporating more details of this molecule. For example, in addition to the simplest futile cycle considered here, other more complicated futile cycles (see, e.g., [22]) can be added into the model; the negative feedback mechanism of $[D]$ on the synthesis of ATP, i.e., the inhibition of ADP binding rate by its high concentration [8], is also not included. Moreover, the continuous motion of the γ rotation has not been explicitly taken into account, as our model simply divides the γ shaft into several discrete states. More comprehensive models incorporating these details will allow us to reveal more hidden mechanistic details of this critical motor protein.

ACKNOWLEDGMENTS

The authors would like to thank Biswajit Das, Xiao Jin, and Ziqing Zhao for comments and helpful discussions. H.G. is supported by National Natural Science Foundation of China (Grants No. 21373021 and No. 11622101) and the 863 program in China (Grant No. 2015AA020406).

[1] P. Boyer, Annu. Rev. Biochem. **66**, 717 (1997).
[2] M. Yoshida, E. Muneyuki, and T. Hisabori, Nat. Rev. Mol. Cell Bio. **2**, 669 (2001).
[3] P. Mitchell, Nature **191**, 144 (1961).
[4] P. Boyer, Angew. Chem. Int. Ed. **37**, 2296 (1998).

[5] W. Junge, H. Sielaff, and S. Engelbrecht, Nature (London) **459**, 364 (2009).
[6] J. Weber and A. E. Senior, Biochim. Biophys. Acta **1458**, 300 (2000).
[7] K. Kinosita, R. Yasuda, and H. Noji, Essays Biochem. **35**, 3 (2000).
[8] K. Kinosita, K. Adachi, and H. Itoh, Annu. Rev. Biophys. Biomol. Struct. **33**, 245 (2004).
[9] R. Yasuda, H. Noji, K. Kinosita, and M. Yoshida, Cell **93**, 1117 (1998).
[10] Y. Rondelez, G. Tresset, T. Nakashima, Y. Kato-Yamada, H. Fujita, S. Takeuchi, and H. Noji, Nature (London) **433**, 773 (2005).
[11] R. Yasuda, H. Noji, M. Yoshida, K. Kinosita, and H. Itoh, Nature (London) **410**, 898 (2001).
[12] T. Ariga, E. Muneyuki, and M. Yoshida, Nat. Struct. Mol. Biol. **14**, 841 (2007).
[13] H. Itoh, A. Takahashi, K. Adachi, H. Noji, R. Yasuda, M. Yoshida, and K. Kinosita, Jr., Nature (London) **427**, 465 (2004).
[14] S. Toyabe, T. Watanabe-Nakayama, T. Okamoto, S. Kudo, and E. Muneyuki, Proc. Natl. Acad. Sci. USA **108**, 17951 (2011).
[15] K. Adachi, R. Yasuda, H. Noji, H. Itoh, Y. Harada, M. Yoshida, and K. Kinosita, Proc. Natl. Acad. Sci. USA **97**, 7243 (2000).
[16] H. Noji, M. Yoshida, and K. Kinosita, Nature (London) **386**, 299 (1997).
[17] H. Omote, N. Sambonmatsu, K. Saito, Y. Sambongi, A. Iwamoto-Kihara, T. Yanagida, Y. Wada, and M. Futai, Proc. Natl. Acad. Sci. USA **96**, 7780 (1999).
[18] H. Wang and G. Oster, Nature (London) **396**, 279 (1998).
[19] Y. Q. Gao, W. Yang, and M. Karplus, Cell **123**, 195 (2005).
[20] L. Xu, Biochim. Biophys. Acta **1777**, 1422 (2008).
[21] O. Pänke and B. Rumberg, Biochim. Biophys. Acta **1412**, 118 (1999).
[22] P. Gaspard and E. Gerritsma, J. Theor. Biol. **247**, 672 (2007).
[23] T. Schmiedl and U. Seifert, Europhys. Lett. **83**, 30005 (2008).
[24] K. Adachi, K. Oiwa, T. Nishizaka, S. Furuike, H. Noji, H. Itoh, M. Yoshida, and K. Kinosita, Cell **130**, 309 (2007).
[25] R. Watanabe, D. Okuno, S. Sakakihara, K. Shimabukuro, R. Iino, M. Yoshida, and H. Noji, Nat. Chem. Biol. **8**, 86 (2012).
[26] R. Watanabe, K. Hayashi, H. Ueno, and H. Noji, Biophys. J. **105**, 2385 (2013).
[27] T. Elston, H. Wang, and G. Oster, Nature (London) **391**, 510 (1998).
[28] See Supplemental Material at http://link.aps.org/supplemental/10.1103/PhysRevE.95.052413 for the details of the model including the equations for each portion of the $F_o F_1$-ATPase, the estimated parameter values and the consistency of the coupled model based on experimental literatures, the results via another F_1 model, and the results in the case of mismatch between F_o and F_1.
[29] X.-J. Zhang, H. Qian, and M. Qian, Phys. Rep. **510**, 1 (2012).
[30] H. Ge and H. Qian, Phys. Rev. E **87**, 062125 (2013).
[31] T. Hill, *Free Energy Transduction and Biochemical Cycle Kinetics* (Springer-Verlag, New York, 1995).
[32] M. E. Fisher and A. B. Kolomeisky, Proc. Natl. Acad. Sci. USA **96**, 6597 (1999).
[33] H. Qian, Biophys. Chem. **83**, 35 (2000).
[34] P. Hänggi, P. Talkner, and M. Borkovec, Rev. Mod. Phys. **62**, 251 (1990).
[35] H.-X. Zhou, Q. Rev. Biophys. **43**, 219 (2010).
[36] E. Saita, T. Suzuki, K. Kinosita, and M. Yoshida, Proc. Natl. Acad. Sci. USA **112**, 9626 (2015).
[37] D. Chowdhury, Phys. Rep. **529**, 1 (2013).
[38] A. E. Senior, S. Nadanaciva, and J. Weber, Biochim. Biophys. Acta **1553**, 188 (2002).
[39] N. Sakaki, R. Shimo-Kon, K. Adachi, H. Itoh, S. Furuike, E. Muneyuki, M. Yoshida, and K. Kinosita, Biophys. J. **88**, 2047 (2005).
[40] S. Toyabe and E. Muneyuki, New J. Phys. **17**, 015008 (2015).
[41] D. Stock, C. Gibbons, I. Arechaga, A. G. Leslie, and J. E. Walker, Curr. Opin. Struct. Biol. **10**, 672 (2000).
[42] W. Jiang, J. Hermolin, and R. H. Fillingame, Proc. Natl. Acad. Sci. USA **98**, 4966 (2001).
[43] E. R. Kashet, Biochemistry **21**, 5534 (1982).
[44] M. K. Al-Shawi, C. J. Ketchum, and R. K. Nakamoto, Biochemistry **36**, 12961 (1997).
[45] J. C. Wilks and J. L. Slonczewski, J. Bacteriol. **189**, 5601 (2007).
[46] G. Oster and H. Wang, J. Bioenerg. Biomem. **32**, 459 (2000).
[47] S. C. Kou, B. J. Cherayil, M. Wei, B. P. English, and X. S. Xie, J. Phys. Chem. B **109**, 19068 (2005).
[48] I. B. Dodd, M. A. Micheelsen, K. Sneppen, and G. Thon, Cell **129**, 813 (2007).
[49] W. Ma, A. Trusina, H. El-Samad, W. A. Lim, and C. Tang, Cell **138**, 760 (2009).
[50] L. Zhang, K. Radtke, L. Zheng, A. Q. Cai, T. F. Schilling, and Q. Nie, Mol. Syst. Biol. **8**, 613 (2012).
[51] S. Chong, C. Chen, H. Ge, and X. S. Xie, Cell **158**, 314 (2014).